Environ Earth Sci
DOI 10.1007/s12665-014-3660-4

ORIGINAL ARTICLE

Effects of slope orientation on pedogenesis of altimontane soils from the Brazilian semi-arid region (Baturité massif, Ceará)

Wesley Rocha Barbosa · Ricardo Espíndola Romero · Valdomiro Severino de Souza Júnior · Miguel Cooper · Lucas Resmini Sartor · Carmen Silvia de Moya Partiti · Fábio de Oliveira Jorge · Renato Cohen · Sérgio Luis de Jesus · Tiago Osório Ferreira

Received: 30 March 2014 / Accepted: 22 August 2014

Abstract Given the importance of climate conditions for the development of soils, studies on climosequences are a valuable tool to predict the influence of climate change on weathering rates and on soil formation processes. The Baturité massif, a humid enclave located in the Brazilian semi-arid region, has unique characteristics that cause a disproportional distribution of rainfall: the eastern and northern slopes receive more than 1,600 mm/year of rainfall, whereas the southern and western slopes have semi-arid characteristics with rainfall of less than 600 mm/year. Eight soil profiles were selected to investigate the influence of these distinct climates on soil formation. To achieve this, physical, chemical, morphological, mineralogical and micromorphological data were determined and analyzed. In the humid slope predominate soil processes include melanization, brunification, intense leaching, acidification and alitization, with intensified weathering in higher altitudes. In contrast, the environment in the dry slope favored the occurrence of soils with a higher base status, high-activity clays, low Al saturation and bisialitization processes coexisting with monosialitization, mainly in the soils located at lower altitudes. Micromorphological data indicate that clay illuviation is not the main process responsible for the enrichment of clay in the subsurface horizons. The contrasting environmental conditions with different mineralogical composition seem to be an important indicator of weathering intensity and pedoenvironmental conditions.

Keywords Altitudinal gradient · Chemical weathering · Pedogenesis · Tropical soils

W. R. Barbosa · R. E. Romero
Departamento de Ciências do Solo, Universidade Federal do Ceará (CCA/UFC), Av. Mister Hull s/n, Fortaleza, Ceará CEP 60021-970, Brazil

V. S. de Souza Júnior
Departamento de Agronomia, Universidade Federal Rural de Pernambuco (UFRPE), Rua Dom Manoel de Medeiros s/n, Recife, Pernambuco CEP 52171-900, Brazil

M. Cooper · L. R. Sartor · T. O. Ferreira (✉)
Departamento de Ciência do Solo, Universidade de São Paulo (ESALQ/USP), Av. Pádua Dias 11, Piracicaba, São Paulo CEP 13418-900, Brazil
e-mail: toferreira@usp.br

C. S. de Moya Partiti · F. O. Jorge · R. Cohen
Instituto de Física, Universidade de São Paulo (IF/USP), Rua do Matão Travessa R 187, São Paulo, São Paulo CEP 05508-090, Brazil

S. L. de Jesus
Núcleo de Pesquisa em Geoquímica e Geofísica da Litosfera, Universidade de São Paulo (NUPEGEL/USP), Av. Pádua Dias 11, Piracicaba, São Paulo CEP 13418-900, Brazil

Introduction

Climate issues have been on the spotlight of the current scientific context for the past years and have aroused interest regarding the effects that climate changes may have on soil evolution (Egli et al. 2009). Those changes may promote abrupt modifications in the intensity of active weathering and pedogenetic processes.

Studies in regions of altitudinal gradient, characterized by decreasing temperatures and increasing rainfalls, have shown the influence of the climatic contrast on soil attributes, such as acidity, clay content, exchangeable cations and soil organic matter (Bockheim et al. 2000; Rech et al. 2001). Although many studies on altimontane soils were performed in high-altitude regions, marked by mild and alpine climates (Bockheim et al. 2000; Rech et al. 2001;

Published online: 04 September 2014

Egli et al. 2009), some studies have aimed to evaluate soil evolution in arid and semi-arid regions (Yousefifard et al. 2012; Brock-Hon et al. 2012).

In general, soils formed in tropical climates are strongly weathered, with deep soil composed of stable secondary minerals (Furian et al. 2002). The humid climate intensifies losses of alkali, alkali-earth elements and silicon and, thus, the formation of kaolinite, oxide and oxyhydroxide minerals. In contrast, in environments under dryer climates, such as semi-arid or arid environments, the soils are mostly poorly to moderately developed and marked by the occurrence of bisialitization and monosialitization processes (Barbiéro et al. 2001; Khormali and Ajami 2011). Yousefifard et al. (2012), studying soil weathering in a semi-arid region from Iran, verified that most soils are formed mainly by physical weathering of bedrock, and that clay minerals are minor constituents in these soils. Climate is responsible for the occurrence of poorly to moderately developed soils, due to the lower intensity of weathering and mobilization of major elements. In this context, studies on sequences of soils developed in contrasting climate environments may be a valuable tool to predict the influence of climate on weathering rates, soil evolutionary stage, and soil formation processes (Egli et al. 2006; Bétard et al. 2007; Egli et al. 2008).

In northeastern Brazil, the semi-arid occupies a total area of about 750,000 km^2 (Ab'Saber 1977). In these macro-region, the predominant vegetation, called caatinga, stands out as one of the main ecosystems of the Brazil, covering an area of about 600,00 km^2 (Sampaio 1995). The Brazilian semi-arid region is one of the most vulnerable to desertification (Souza et al. 2012) and periodic droughts (Silva 2004).

Contrasting with this semi-arid scenario, the humid sierras stand out as climatic exceptions. These ranges of mountains with medium altitudes (600–1,200 m) act as orogenic barriers to the wet fronts of air coming from the Atlantic Ocean. These mountainous obstacles favor the occurrence of high orographic rainfalls (1,200-2,000 mm/year), constituting true "islands of humidity" characterized by the presence of evergreen forest fragments within a harsh semi-arid (Bétard et al. 2007). Among these singular semi-arid environments is the Baturité massif, a geomorphological feature that spreads over an area of 3,580 km^2 in the state of Ceará (NE Brazil).

Due to the importance, peculiarity and the lack of information on the diversity of soils in the Brazilian altimontane environments, especially those occurring in semi-arid regions, a study was carried out aiming to evaluate the effects of the climate contrast on the pedogenesis of its soils. For this, physical, chemical, morphological, mineralogical and micromorphological data of an altitudinal sequence of eight soil profiles were determined and discussed. The objectives of this work are (i) to characterize the physical, chemical, macromorphological, micromorphological and mineralogical aspects of altimontane soils; (ii) evaluate the influence of contrasting climatic conditions on degree of weathering and pedogenetic evolution of altimontane soils from the Brazilian semi-arid region.

Materials and methods

Study area

The Baturité massif is located in the northern part of the Ceará state, about 50 km from the coast line (Fig. 1) and occupies 2.4 % of the area of Ceará (Souza 1994). From a geomorphological perspective, the Baturité massif is located within the domain of the Residual Massifs. These geologic formations are the result of the higher resistance of the lithotypes of the massif under weathering and pediplanation of the surrounding areas, which occurred in previous, drier periods. Thus, the Baturité massif can be considered a vast residual relief, preserved above a leveling surface and denominated by depressão sertaneja (Bétard et al. 2007). From a lithological perspective, the Baturité massif consists almost entirely of rocks from the crystalline basement from the Precambrian Era (Jacomine et al. 1973), showing a petrography basically dominated by gneisses and migmatites.

The average monthly temperatures in the region range from 20 to 22 °C at the highest altitudes, where the temperature range does not exceed 2 °C. Temperatures increase at the lower altitudes, reaching monthly averages of more than 26 °C (Souza 1994). The humid portion of the massif, delineated by the northern and eastern slopes, shows a tropical monsoon climate (Amw'), while the southern and western slopes show a dry, semi-arid climate (BSw'h').

The humid portion of the massif is characterized by the occurrence of high orographic rainfalls (1,200–2,000 mm/year), caused by the range of mountains with medium altitudes (600–1,200 m) acting as orogenic barriers to wet fronts of air from the Atlantic Ocean. In contrast, the southern and western slopes have semi-arid characteristics, with annual precipitation that remains below 600 mm/year, constituting a "rain shadow" environment. The rainy season in both areas of the massif are concentrated in few months; in the humid zone, the dry season lasts less than 5 months, while in the dry zone it can last 10 months.

Consistent with the climatic contrast, the vegetation of the massif shows a clear zonation, with the following units: (i) Primary evergreen forest (Atlantic rainforest), located above the altitude of 900 m; (ii) Semi-evergreen forest,

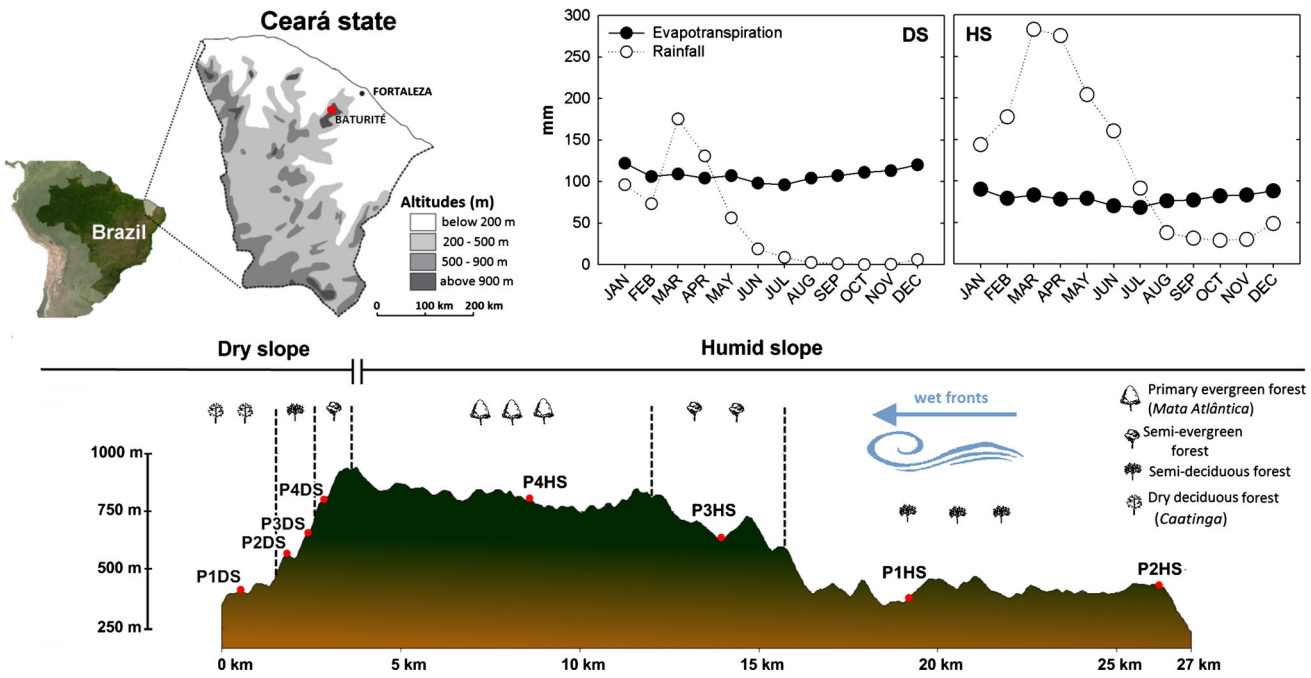

Fig. 1 Location of studied soil profiles (Baturité massif, Ceará, Brazil)

located between 600 and 800 m; (iii) Semi-deciduous forest, located at altitudes between 400 and 800 m; (iv) Dry deciduous forest (Caatinga), located on the foothills or at the lowest elevations.

Sample collection

Soil sampling and description were performed on two opposite slopes on the Baturité Massif, one located on the northern side of the Massif and the other on its eastern side, representing, respectively, the humid slope (HS) and the dry slope (DS). The study was performed along two soil toposequences.

For that, eight soil profiles were described and sampled on each slope (Fig. 1). To rule out the effect of topography as a dominant factor in the formation of the soils, soil profiles were located on sites with flat relief. To facilitate the comparison of soils from the two slopes, the profiles were sampled at nearly the same altitude. All sampled and analyzed soils were located above the altitude of 400 m, within the municipalities of Palmácia, Pacoti and Guaramiranga on the humid slope, and within Caridade on the dry slope.

Laboratory analyses

Soil samples from all horizons were dried, passed through 10 mesh sieves (2 mm grid) and stored for analyses in the laboratory. To determine particle size distribution, the samples underwent a pre-treatment to eliminate organic matter (H_2O_2) and were analyzed through the pipet method (Gee and Bauder 1986), after chemical dispersion with NaOH. To obtain the contents of exchangeable bases (Ca^{2+}, Mg^{2+}, Na^{+} and K^{+}), an extracting solution of ammonium acetate (1 M NH_4OAc) was used, while potential acidity ($H^{+} + Al^{3+}$) was determined with a solution of calcium acetate in pH 7.0 (Quaggio et al. 1985).

To meet the requirements for the Brazilian Soil Classification System (Embrapa Embrapa 2013), 1 g of air-dried soil was dissolved in 20 mL of H_2SO_4 (1:1) and the amounts of SiO_2, Al_2O_3, and Fe_2O_3 were determined in the sulfuric extract (Embrapa 2011). Semi-quantitative estimates of the abundance of secondary mineral phases were calculated using the Ki ratio (1.7 SiO_2/Al_2O_3), a common index that indicates the degree of alteration or weathering in tropical soils. Ki values below 1.0 indicate the predominance of iron oxides and aluminum hydroxide (gibbsite); values close to 2.0 indicate the predominance of kaolinite and values higher than 2.0, the occurrence of 2:1 phyllosilicates (Tardy 1971).

Sodium citrate-bicarbonate-dithionite (CBD) was used to extract pedogenic iron (Fe_d), following a sequence of three successive extractions every 15 min (80 °C) (Mehra and Jackson 1960). To obtain measurements of low-crystallinity iron (Fe_o), ammonium oxalate ($(NH_4)_2C_2O_4{\cdot}H_2O$ at pH 3.0) was used in the absence of light. For total iron determination (Fe_t), extractions with sulfuric attack (H_2SO_4, 1:1) were performed, according to Embrapa

protocol (Embrapa 2011). Determination of elements present was performed using atomic emission spectrometry, with the spectrometer Optima 4300 DV, Perkin Elmer.

To identify minerals in clay fraction, powder diffraction patterns of total clay were performed by X-ray diffraction (XRD). The clay fraction was obtained by decantation in a dispersing solution of sodium hydroxide and was not subjected to any saturation or heating treatment. The diffractograms were generated in intervals of 3–30°2θ and 3–50°2θ for total clay and oxides concentration, respectively, with 2 s/step of 0.02°2θ, using CuKα radiation. Iron oxides from the clay fraction were concentrated using 5 mol L^{-1} NaOH (Kämpf and Schwertmann 1982). For better characterization of the soil mineralogy, Mössbauer spectra were measured with a conventional constant-acceleration spectrometer and a Rh(^{57}Co) source. Absorbers were prepared by pressing finely ground samples between two Lucite plates with a sample thickness of 10 mg cm^{-2} Fe. All Mössbauer measurements were performed at 77 K in a liquid-nitrogen cryostat to minimize magnetic relaxation effects due to small particle of the iron oxides.

Undisturbed samples of different soil horizons were collected for micromorphological studies. All soil samples were dried and the samples were impregnated by capillarity (Murphy 1986) with an unsaturated polyester resin (Polydyne 5061—Cristal) mixed with styrene monomer. The polished blocks were mounted onto glass slides followed by additional polishing to obtain 30 μm thick thin-sections. The micromorphological descriptions were performed using the criteria proposed by Bullock et al. (1985) and Stoops (2003).

Results and discussion

Differences in morphological, chemical and physical attributes of soil profiles

The morphological characteristics and chemical and physical data of the profiles from both slopes were used to classify the soils taxonomically (Tables 1, 2). The classification of the studied profiles was done according to the World Reference Base for Soil Resources (IUSS Working Group WRB 2006) and Soil Taxonomy (Soil Survey Staff 2014). The results of physical and chemical analyses (Tables 1, 2) evidenced clear differences between soils from the opposite slopes, as well as contrasts with respect to the altitudinal gradients. Granulometric data showed that there were no substantial changes regarding textural class between the studied soils, however, some differences in granulometry between soils from both slopes were observed. In general, most soils from both slopes presented a clay-enriched subsoil, with an argic horizon (argillic according to Soil Taxonomy) (except for P4HS), but differed taxonomically, mostly due to chemical attributes (discussed below). All subsurface soil horizons from the HS (329–518 g kg^{-1}; Table 1) showed higher clay contents when compared to those in DS (183–398 g kg^{-1}; Table 1). Additionally, for both slopes the average clay content increased with altitude (from ~400 to ~600 m). These clay distribution patterns seem to indicate that weathering is increased at the HS slope, and that weathering also increases with altitude (at both slopes). This assumption is in accordance with the Ki values, silt/clay ratios and clay activities, which also indicate a more intense weathering environment at the HS. Subsurface horizons from HS soil profiles showed lower Ki index values (1.8–2.2), silt/clay ratios (0.1–0.5) and clay activities (18–26 $cmol_c$ kg^{-1} clay), while higher values were obtained in DS soils (2.2–3.2; 0.4–1.1 and 19–100 $cmol_c$ kg^{-1} clay, respectively for Ki index, silt/clay ratio and clay activity).

In general, soils from the HS presented a moderate to strong acidity ($4 > pH < 6$) and a very low base status (BS < 50 %), with most soil profiles presenting Al saturation values of 50 % or more, especially with increasing altitudes (>600 m; P3HS and P4HS). Contrastingly, soil profiles from the DS presented higher base status (BS > 50 %), high-activity clays (CEC > 24 $cmol_c$ kg^{-1} $clay^{-1}$), and low Al saturation (<50 %), with the exception of P4DS, located above 800 m.

With respect to soil color, surface soil horizons from the DS presented higher value and chroma when compared to HS soil profiles (Table 1). These contrasting colors, marked by lower values and chroma in HS soils, evidence a higher supply of organic matter in this area, probably related to the denser vegetation cover, which supplies the soil surface with higher biomass in response to the more wet conditions (especially at higher altitudes), generating higher TOC contents (Table 2) and a more intense melanization process (darkening of surface soil horizons). In fact, although soils from both slopes have showed increasing TOC contents with higher altitudes, TOC values were always higher in surface horizons from the HS (28.75–42.65 g kg^{-1}) when compared to those from the DS (11.03–32.25 g kg^{-1}; Table 2).

The altitudinal effect on climatic conditions may be evidenced by the similar colors (10YR 3/3 and 10YR 3/4) found in profiles P4HS and P4DS, which, despite being located on opposite sides of the Massif, are probably subjected to similar pedoenvironments, especially with respect to relative humidity. However, despite the proximity between these soil profiles, TOC contents remained higher in the HS (Table 2), evidencing a stronger melanization process.

Table 1 Selected macromorphological and physical characteristics of studied soil profiles

Horizon/depth (cm)	Silt (g kg^{-1})	Clay (g kg^{-1})	Sand (g kg^{-1})	Color (moist)	Textural classes[a]	Structure[b]	Coatings[c]
P1HS (368 m)—Haplic Alisol (Alumic, Rhodic) (Typic Rhodudult)							
A (0–11)	207	207	586	5YR 3/2	scl	f m sbk gr (2)	–
AB (11–30)	158	265	577	7.5YR 3/2	scl	m co sbk (2)	–
BA (30–53)	167	341	491	7.5YR 3/2	scl	m co sbk (2)	–
Bt_1 (53–77)	159	429	413	2.5YR 3/4	c	m co sbk (2)	–
Bt_2 (77–105)	219	360	421	2.5YR 3/4	cl	m co sbk (2)	–
BC (105–193+)	258	143	600	2.5YR 4/6	–	–	–
P2HS (423 m)—Hyperalic Alisol (Chromic) (Typic Hapludult)							
A (0–8)	217	133	650	10YR 3/2	sl	f m co gr 2	–
AB (8–24)	196	201	603	10YR 3/2	scl	f m co gr e sbk (2, 3)	–
BA (24–48)	205	291	504	10YR 4/3	scl	m co sbk (2, 3)	–
Bt_1 (48–59)	191	329	480	5YR 3/3	scl	co sbk (2, 3)	–
Bt_2 (59–83)	185	348	467	5YR 3/2	scl	f m sbk (2)	–
Cr (83–134+)	199	324	477	10YR 3/2	–	–	–
P3HS (658 m)—Haplic Acrisol (Alumic, Clayic) (Typic Hapludult)							
A (0–9)	189	262	549	10YR 3/2	scl	vf f m co gr (3)	–
AB (9–17)	144	253	603	10YR 3/3	scl	vf f m co gr (3)	–
BA (17–29)	203	318	479	10YR 4/4	scl	vf f m sbk (3)	–
Bt_1 (29–50)	121	510	369	7.5YR 4/4	c	vf f m co sbk (3)	–
Bt_2 (50–60)	114	518	368	7.5YR 4/6	c	vf f m co sbk (1, 2, 3)	–
BC (60–91)	109	307	584	–	–	–	–
C (91–180+)	162	216	622	–	–	–	–
P4HS (846 m)—Haplic Cambisol (Alumic, Humic) (Oxic Dystrudept)							
A (0–18)	108	430	463	10YR 3/3	sc	f m sbk gr (2)	–
BA (18–29)	55	483	462	10YR 4/4	sc	f m sbk (2)	–
Bi (29–48)	50	484	466	10YR 4/5	sc	f m sbk (2)	–
BC (48–73)	52	464	484	10YR 4/4	–	m sbk (1)	–
CB (73–118)	43	311	646	2.5YR 4/8	–	–	–
C (118–208+)	100	268	632	2.5 YR 3/6	–	–	–
P1DS (396 m)—Cutanic Luvisol (Epidystric, Rhodic) (Ultic Haplustalf)							
BA (0–29)	194	332	474	7.5YR 4/6	scl	f m sbk (2)	–
Bt_1 (29–50)	224	388	388	5YR 4/6	cl	f m sbk (23)	+
Bt_2 (50–63)	212	306	482	2.5YR 4/6	scl	f sbk (3)	+
BC (63–89)	228	183	590	2.5YR 3/6	–	f sbk (2)	–
CB_1 (89–121)	204	93	702	2.5YR 4/6	–	vf f sbk (2)	–
CB_2 (121–177 +)	236	169	595	7.5YR 4/6	–	f m sbk (2)	–
P2DS (571 m)—Cutanic Luvisol (Hypereutric, Chromic) (Typic Haplustalf)							
A (0–10)	331	180	488	5YR 3/3	l	f m sbk (3)	–
AB (10–20)	297	284	419	2.5YR 4/4	cl	co sbk (3)	–
Bt_1 (20–50)	359	308	333	2.5YR 5/6	cl	co pr (3)	+
Bt_2 (50–75)	318	276	405	7.5YR 5/8	cl	co pr (3)	+
C_1 (75–95)	192	167	641	5YR 3/4	–	–	–
C_3 (125–190+)	222	52	725	10YR 5/6	–	–	–
P3DS (679 m)—Cutanic Luvisol (Hypereutric, Chromic) (Typic Haplustalf)							
A (0–16)	269	196	536	5YR 3/4	sl	m co sbk gr (3)	–
AB (16–30)	261	236	503	7.5YR 4/6	scl	m sbk (3)	–
Bt_1 (30–74)	244	343	414	2.5YR 4/6	cl	m co sbk (2)	+

Table 1 continued

Horizon/depth (cm)	Silt (g kg^{-1})	Clay (g kg^{-1})	Sand (g kg^{-1})	Color (moist)	Textural classes[a]	Structure[b]	Coatings[c]
Bt_2 (74–137)	299	398	303	2.5YR 4/6	cl	ft m co sbk (2)	+
C (137–175 +)	349	121	530	10YR 5/8	–	–	–
P4DS (823 m)—Haplic Acrisol (Chromic) (Typic Haplustult)							
A (0–22)	183	268	549	10YR 3/3	scl	m sbk (3)	–
BA_1 (22–39)	163	334	503	10YR 4/4	scl	f m sbk (3)	–
BA_2 (39–73)	178	335	486	7.5YR 4/4	scl	m co sbk (2)	–
Bt (73–132)	195	313	492	5YR 4/6	scl	m co sbk (2)	–
BC (132–193+)	252	244	504	7.5YR 5/6	–	–	–

[a] Textural classes: sandy clay loam (scl); clay loam (cl); sandy clay (sc); clay (c); sandy loam (sl); loam (l)

[b] Structure (type/size/grade): subangular blocky (sbk); granular (gr); very fine (vf); fine (f); medium (m); coarse (co); prismatic (pr); weak (1); moderate (2); strong (3)

[c] Coatings: absent (−); present (+)

Soil colors registered in subsurface horizons from both slopes also evidenced contrasting pedoenvironments. Hue from B horizons in the humid slope indicates the dominance of yellowish colors (5YR and 10YR) and, thus, the occurrence of brunification. Brunification involves the release of iron from primary minerals followed by the formation of goethite, which is readily bound with organic compounds, giving the soil brownish colors. Thus, brunification is more likely to occur in conditions of low temperate, high moisture and moderate acidity, in which organic matter has higher participation (Kämpf and Schwertmann 1982; Kaiser and Guggenberger 2007).

As for the DS, the 2.5YR hue was prevalent in its soils, indicating the presence of reddish colors. Reddish colors indicate the occurrence of hematite and, also, the rubification process (the development of red color in soils or reddening) which is favored by low humidity, warm temperatures, and rapid turnover of organic matter (Boero and Schwertmann 1989; Chen et al. 2010).

This scenario is consistent with the conditions at the DS where precipitation is significantly lower and temperatures are higher. In this pedoenvironment, organic matter is rapidly decomposed and iron is not readily complexed, resulting in hematite formation through dehydration of ferrihydrite. In fact, Torrent et al. (1982), Schwertmann (2008) and Etame et al. (2009) pointed out that, under higher temperatures and lower water activity conditions, both the instability and dehydration of ferrihydrite are favored, resulting in transformation into hematite.

Weathering intensity and secondary minerals

The XRD patterns of the iron-concentrated clay samples (Fig. 2a and b) show some differences between the humid and dry slopes, in accordance with the process involved in iron mineral formation. Based on the XRD peak intensities, goethite seems to prevail in all soil profiles, however, with higher intensity peaks in the HS soil profiles. On the other hand, the more intense hematite XRD peaks were observed in soil profiles from the DS. These results indicate the dominance of brunification and goethite genesis in the HS soils profiles, contrasting with the rubification processes and hematite formation in DS soils. It should also be noted, however, that the altitudinal gradient (both increasing and decreasing) caused different patterns in both slopes. For example, the P4DS profile, despite of its location within the DS, showed yellowish colors and more intense XRD peaks (relative to goethite), which could be attributed to its location on a higher altitudinal zone ($\sim$800 m) and, thus, under a similar pedoenvironment to that of P4HS. Similarly, the reddish colors (2.5YR) and more pronounced hematite peaks (33.0°, 35.5° and 49.2°2θ) observed in P1HS are consistent with its transitional position between the semi-deciduous forest to the dry caatinga deciduous forest (i.e., between a more humid and a more arid condition).

The lower Fe_d−Fe_o values in surface horizons from all studied profiles (irrespective of slope) provide further evidence for the iron complexation by organic matter (Table 2). Schwertmann(1966), Oliveira et al. (2010) stated that organic matter acts as a complexant, and that this process can inhibit iron oxide crystallization and favor the occurrence of greater amounts of less crystalline iron (Fe_o), with respect to more crystalline iron forms (Fe_d).

The Mössbauer spectroscopy data, measured at 77 K (Fig. 3 and Table 3), were generated to better characterize the iron mineral phases in the studied soils. Intense central doublets were evident and related to the iron oxyhydroxides and/or within phyllosilicates. The spectra revealed goethite as the dominant iron oxide in the soils, with a

Table 2 Chemical and iron selective dissolution analysis of studied soil profiles

Horizon/ depth (cm)	TOC ($g\ kg^{-1}$)	pH (H_2O)	Na^+ ($cmol_c\ kg^{-1}$)	Ca^{2+} ($cmol_c\ kg^{-1}$)	Mg^{2+} ($cmol_c\ kg^{-1}$)	K^+ ($cmol_c\ kg^{-1}$)	H + Al ($cmol_c\ kg^{-1}$)	Al^{3+} ($cmol_c\ kg^{-1}$)	S ($cmol_c\ kg^{-1}$)	CEC ($cmol_c\ kg^{-1}$)	BS (%)	Sat. Al^{3+} (%)	Ki	Fe_t ($g\ kg^{-1}$)	Fe_o ($g\ kg^{-1}$)	Fe_d ($g\ kg^{-1}$)	$Fe_d - Fe_o$ ($g\ kg^{-1}$)
P1HS (368 m)—Haplic Alisol (Alumic, Rhodic) (Typic Rhodudult)																	
A (0–11)	42.65	6.71	0.14	6.30	2.40	0.21	4.95	0.30	9.05	14.01	65	3	2.33	25.29	3.03	17.17	14.14
AB (11–30)	15.07	5.52	0.06	1.10	1.40	0.39	6.69	1.40	2.95	9.64	31	32	2.67	27.26	3.52	24.04	20.52
BA (30–53)	12.84	5.35	0.07	1.70	0.90	0.28	9.41	3.20	2.95	12.37	24	52	0.58	39.60	3.55	34.53	30.98
Bt_1 (53–77)	11.67	5.20	0.07	1.00	1.70	0.18	7.93	2.20	2.95	10.87	27	43	0.42	57.89	3.59	47.27	43.68
Bt_2 (77–105)	9.02	5.19	0.07	0.80	2.10	0.14	5.70	1.50	3.11	8.81	35	33	2.0	58.85	2.49	56.57	54.08
BC (105–193+)	5.94	5.33	0.08	1.20	1.10	0.07	4.95	4.30	2.45	7.40	33	64	2.07	51.21	2.05	43.82	41.77
P2HS (423 m)—Hyperalic Alisol (Chromic) (Typic Hapludult)																	
A (0–8)	28.75	5.33	0.05	1.50	1.40	0.47	7.18	1.00	3.42	10.60	32	23	2.47	5.48	2.24	3.64	1.40
AB (8–24)	14.43	5.10	0.04	0.70	0.50	0.33	5.70	2.90	1.57	7.26	22	65	2.35	8.79	2.84	4.59	1.75
BA (24–48)	9.02	5.31	0.05	0.80	0.60	0.26	10.41	4.20	1.71	12.11	14	71	2.2	10.97	2.19	5.39	3.20
Bt_1 (48–59)	9.34	5.40	0.06	1.00	1.00	0.23	6.44	3.10	2.29	8.73	26	58	2.26	12.03	2.09	6.42	4.33
Bt_2 (59–83)	7.64	5.33	0.06	1.00	1.40	0.17	5.95	3.10	2.63	8.57	31	54	0.06	14.38	1.44	6.44	5.00
Cr (83–134+)	5.09	5.14	0.06	1.80	0.90	0.14	4.95	2.50	2.90	7.85	37	46	1.58	14.37	1.58	6.56	4.98
P3HS (658 m)—-Haplic Acrisol (Alumic, Clayic) (Typic Hapludult)																	
A (0–9)	46.04	4.68	0.06	2.30	1.20	0.37	12.64	2.80	3.93	16.57	24	42	2.16	21.96	3.38	8.64	5.26
AB (9–17)	21.11	4.55	0.04	1.10	0.80	0.22	9.17	4.30	2.16	11.33	19	67	0.8	21.54	2.98	18.86	15.88
BA (17–29)	15.91	4.68	0.06	0.90	1.00	0.23	8.67	3.90	2.19	10.86	20	64	0.67	26.82	3.47	24.57	21.10
Bt_1 (29–50)	14.32	5.05	0.06	1.00	0.60	0.21	7.43	6.20	1.87	9.30	20	77	0.39	46.15	2.84	38.91	36.07
Bt_2 (50–60)	10.50	5.02	0.06	0.80	0.70	0.17	7.43	6.50	1.73	9.16	19	79	2.08	47.60	0.58	43.82	43.24
BC (60–91)	6.58	5.13	0.08	0.90	0.40	0.13	5.70	5.10	1.51	7.20	21	77	1.93	36.91	1.07	37.45	36.38
C (91–180+)	6.15	5.25	0.07	1.40	0.50	0.12	6.44	6.80	2.09	8.53	25	76	1.73	56.38	1.09	39.04	37.95
P4HS (846 m)—Haplic Cambisol (Alumic, Humic) (Oxic Dystrudept)																	
A (0–18)	43.71	4.79	0.06	0.40	0.20	0.17	16.60	7.10	0.83	17.43	5	89	1.86	30.14	2.43	32.36	29.93
BA (18–29)	18.57	4.91	0.04	0.30	0.00	0.05	10.16	8.80	0.39	10.55	4	96	1.77	33.14	1.59	42.23	40.64
Bi (29–48)	17.82	4.90	0.04	0.20	0.00	0.05	9.91	7.00	0.29	10.19	3	96	0.41	34.38	1.64	41.17	39.53
BC (48–73)	14.75	4.84	0.02	0.20	0.00	0.03	8.92	6.60	0.25	9.17	3	96	1.81	33.88	1.20	43.03	41.83
CB (73–118)	6.15	4.80	0.02	0.10	0.00	0.02	3.96	3.80	0.13	4.09	3	97	0.62	27.89	0.59	32.14	31.55
C (118–208+)	5.09	4.70	0.02	0.20	0.00	0.02	2.97	3.80	0.23	3.20	7	94	1.73	28.33	0.57	35.99	35.42
P1DS (396 m)—Cutanic Luvisol (Epidystric, Rhodic) (Ultic Haplustalf)																	
BA (0–29)	11.03	4.76	0.09	1.50	0.30	0.20	8.67	8.20	2.08	10.75	19	80	2.53	40.45	2.07	33.09	31.02
BA_2 (29–50)	7.64	5.03	0.10	1.40	1.20	0.20	7.68	6.80	2.90	10.58	27	70	1.86	46.50	3.00	41.96	38.96
Bt_1 (50–63)	5.84	5.16	0.08	1.30	2.70	0.17	4.71	3.20	4.25	8.95	47	43	1.88	42.13	3.21	51.13	47.92

Table 2 continued

Horizon/ depth (cm)	TOC ($g\ kg^{-1}$)	pH (H_2O)	Na^+ ($cmol_c\ kg^{-1}$)	Ca^{2+} ($cmol_c\ kg^{-1}$)	Mg^{2+} ($cmol_c\ kg^{-1}$)	K^+ ($cmol_c\ kg^{-1}$)	H + Al ($cmol_c\ kg^{-1}$)	Al^{3+} ($cmol_c\ kg^{-1}$)	S ($cmol_c\ kg^{-1}$)	CEC ($cmol_c\ kg^{-1}$)	BS (%)	Sat. Al^{3+} (%)	Ki	Fe_t ($g\ kg^{-1}$)	Fe_o ($g\ kg^{-1}$)	Fe_d ($g\ kg^{-1}$)	$Fe_d - Fe_o$ ($g\ kg^{-1}$)
Bt_2 (63–89)	6.58	5.19	0.09	1.80	2.20	0.14	3.96	3.30	4.22	8.19	52	44	2.22	60.20	2.83	50.59	47.76
CB_1 (89–121)	4.99	5.13	0.09	1.50	2.50	0.16	3.22	1.60	4.25	7.47	57	27	0.44	35.17	2.05	36.12	34.07
CB_2 (121–177+)	4.03	4.84	0.16	2.50	1.80	0.31	2.73	2.60	4.77	7.50	64	35	1.85	57.59	1.48	30.28	28.80
P2DS (571 m)—Cutanic Luvisol (Hypereutric, Chromic) (Typic Haplustalf)																	
A (0–10)	32.25	7.40	0.10	13.8	0.20	0.72	2.23	0.30	14.8	17.05	87	2	2.83	33.99	3.30	13.00	9.70
AB (10–20)	16.55	6.34	0.21	14.6	1.30	0.40	4.46	0.10	16.5	20.97	79	1	0.65	41.20	2.75	9.62	6.87
Bt_1 (20–50)	7.96	6.70	0.33	28.1	0.40	0.30	3.72	0.50	29.1	32.84	89	2	2.59	48.79	1.57	30.18	28.61
Bt_2 (50–75)	5.09	6.83	0.34	34.5	1.40	0.24	3.22	1.10	36.4	39.69	92	3	3.27	54.23	1.03	11.70	10.67
C_1 (75–95)	4.14	6.97	0.26	19.8	2.30	0.24	2.48	0.20	22.5	25.07	90	1	3.03	38.14	1.68	16.40	14.72
C_3 (125–190+)	2.12	7.21	0.39	38.0	4.82	0.16	1.98	1.30	43.4	45.43	96	3	3.73	46.64	3.23	15.80	12.57
P3DS (679 m)—Cutanic Luvisol (Hypereutric, Chromic) (Typic Haplustalf)																	
A (0–16)	30.85	6.50	0.08	6.40	2.90	0.56	4.46	0.30	9.94	14.40	69	3	2.79	39.30	7.76	24.85	17.09
AB (16–30)	14.22	6.82	0.08	5.60	3.70	0.21	3.72	0.20	9.59	13.30	72	2	2.73	44.41	8.61	37.64	29.03
Bt_1 (30–74)	8.28	6.35	0.14	8.80	2.60	0.16	4.46	0.20	11.7	16.15	72	2	2.57	56.65	6.87	37.23	30.36
Bt_2 (74–137)	5.84	6.41	0.38	11.2	7.40	0.17	3.96	0.40	19.1	23.12	83	2	1.93	68.70	5.00	41.03	36.03
C (137–175+)	3.61	6.75	0.58	15.5	4.40	0.09	3.22	0.60	20.6	23.78	86	3	3.17	85.99	6.69	19.97	13.28
P4DS (823 m)—Haplic Acrisol (Chromic) (Typic Haplustult)																	
A (0–22)	31.19	6.88	0.06	6.00	1.10	0.82	3.72	0.50	7.98	11.70	68	6	1.35	26.41	2.61	24.17	21.56
BA_1 (22–39)	14.64	5.87	0.05	1.50	0.90	0.32	5.20	1.10	2.76	7.97	35	28	1.58	32.40	2.73	32.14	29.41
BA_2 (39–73)	7.21	5.42	0.03	1.30	0.80	0.24	7.43	0.40	2.37	9.80	24	14	1.89	35.81	0.93	33.73	32.80
Bt (73–132)	4.56	5.37	0.05	1.40	0.70	0.29	3.72	0.90	2.43	6.15	40	27	2.3	37.26	0.95	41.43	40.48
BC (132–193+)	3.61	5.69	0.06	1.20	0.90	0.34	3.22	0.60	2.50	5.72	44	19	2.03	48.70	0.83	46.88	46.05

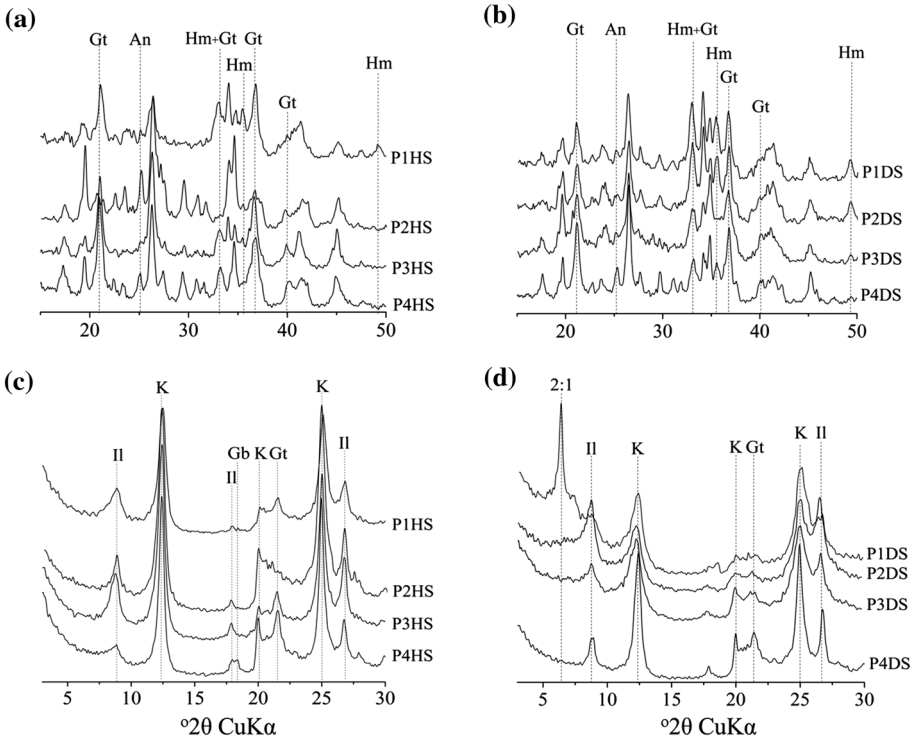

Fig. 2 XRD patterns of concentrate oxides from diagnostic horizons (**a** and **b**) and clay fraction (**c** and **d**). *K* Kaolinite, *Il* illite, *Hm* hematite, *Gt* goethite, *An* anatase, *2:1* expandable clay

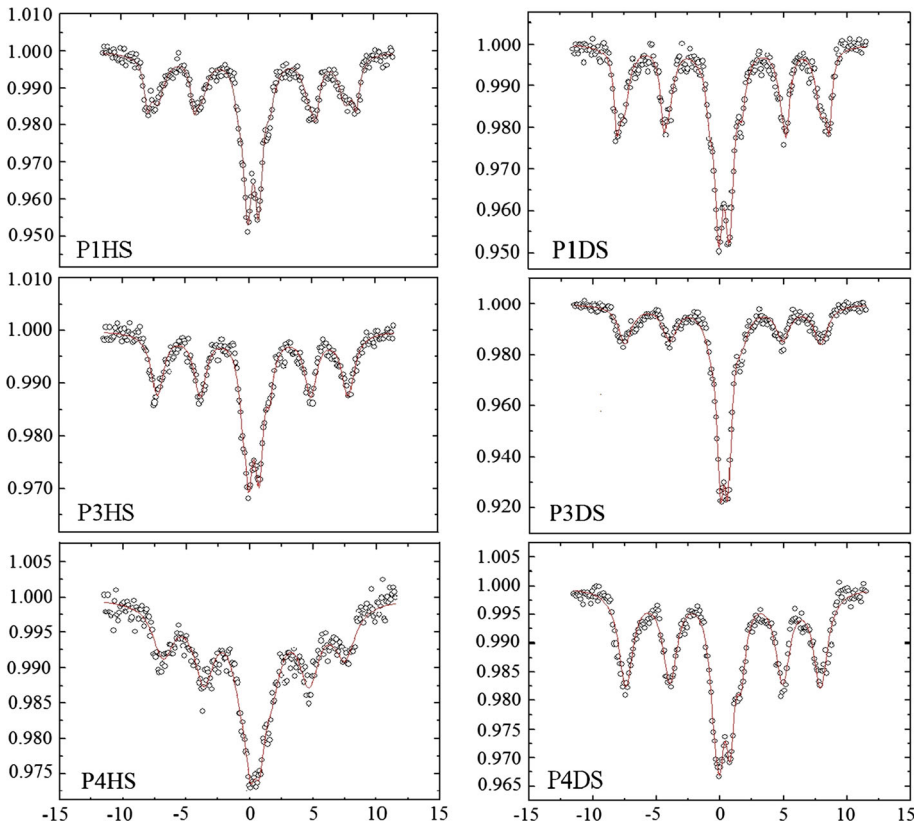

Fig. 3 Mössbauer spectra of studied B horizon from soil profiles

Table 3 Mössbauer parameters of studied soil profiles

Phase	B_{hf} (T)	Δ (mm s^{-1})	δ (mm s^{-1})	Ar (%)
P1HS (368 m)—Haplic Alisol (Alumic, Rhodic) (Typic Rhodudult)				
Gt	46.1 (2)	−0.31 (3)	0.54 (1)	46
Hm	51.3 (1)	−0.19 (1)	0.51 (1)	19
Fe^{3+}	–	0.87 (1)	0.52 (1)	35
P3HS (658 m)—Haplic Acrisol (Alumic, Clayic) (Typic Hapludult)				
Gt	46.7 (1)	−0.25 (2)	0.55 (1)	63
Fe^{3+}	–	0.81 (2)	0.50 (3)	33
Fe^{2+}	–	2.11 (6)	0.67 (1)	4
P4HS (846 m)—Haplic Cambisol (Alumic, Humic) (Oxic Dystrudept)				
Gt	44.3 (3)	−0.20 (5)	0.54 (3)	82
Fe^{3+}	–	0.67 (5)	0.53 (2)	18
P1DS (396 m)—Cutanic Luvisol (Epidystric, Rhodic) (Ultic Haplustalf)				
Gt	47.8 (2)	−0.25 (3)	0.51 (1)	40
Hm	51.4 (1)	−0.19 (1)	0.46 (1)	23
Fe^{3+}	–	0.81 (1)	0.44 (1)	37
P3DS (679 m)—Cutanic Luvisol (Hypereutric, Chromic) (Typic Haplustalf)				
Gt	47.7 (1)	−0.26 (2)	0.48 (1)	56
Fe^{3+}	–	0.57 (1)	0.45 (1)	44
P4DS (823 m)—Haplic Acrisol (Chromic) (Typic Haplustult)				
Gt	47.4 (1)	−0.24 (2)	0.51 (1)	66
Fe^{3+}	–	0.83 (1)	0.51 (1)	26
Fe^{2+}	–	2.11 (3)	0.74 (1)	8

Gt Goethite, *Hm* hematite, Fe^{3+} high spin octahedral coordination, B_{hf} hyperfine field, Δ quadrupole splitting, δ isomeric shift, *Ar* relative area

certain degree of isomorphic substitution, shown by the low values of hyperfine fields that were expected for this mineral (maximum of 48.1 T). In addition, hematite and possible traces of ferrihydrite were identified as constituents of the soil's profile by their characteristic parameters (Table 3), given that in some cases no magnetic order is observed for ferrihydrite, even at 4.2 K (Schwertmann et al. 2005).

The values of the hyperfine fields related to goethite were always lower in the humid slope, ranging from 44.3 (P4HS) to 46.7 T (P3HS), making clear that the goethite present in the soils located in the humid slope has a higher degree of isomorphic substitution. This is another indicator that the soils of the HS are more weathered than in the DS, which can be explained by higher aluminum activity in the HS, which promotes the substitution of iron for aluminum in the goethite crystal lattice (Fitzpatrick and Schwertmann 1982; Motta and Kämpf 1992). This result agrees with the XRD data, which showed predominant goethite features in most soils. Similarly, for P1HS and P1DS, the spectra presented hematite patterns, with hyperfine field values around 51.4 T, also agreeing with the XRD patters. High quadrupole splitting suggests the presence of relatively high amounts of Fe^{2+} in the illite structure, due to the distortion of the octahedral sites (Murad and Wagner 1994); this can be an indicator of transformation processes of biotite into illite.

It was also observed that soil profiles located at higher altitudes showed higher values of relative goethite area than others, with relative area (RA) of 83 and 66 % for P4HS and P4DS, respectively. Accordingly, P1HS and P1DS profiles, located at lower altitudes, were the only profiles that showed clear hematite patterns in the spectra, confirming the more favorable conditions for hematite formation relative to goethite. These results agree with XRD and morphological data, which show more intense peaks for goethite and a predominance of 10YR hue in this soil (P4HS and P4DS), as well as XDR patters of hematite on the profiles located on lower altitudes (P1HS e P1DS). Besides the more crystalline iron oxides (goethite and hematite), Fe^{3+} doublets suggest the presence of ferrihydrite in the soils, since no orientation was observed at 77 K. However, for more reliable interpretations, data collection under cryogenic conditions (4.2 K) is needed, to block paramagnetic relaxation and improve the spectral resolution.

Although the clay fraction XRD patterns of soils have evidenced similar mineral assemblages in both slopes (dominance of illite and kaolinite), the existence of contrasting weathering environments (Fig. 2c and d) is also supported. Illite was confirmed by XRD peaks in the angle of 8.7°2θ, while kaolinite showed its XRD peaks in 12.3°2θ (Moore and Reynolds 1997). Within the HS, gibbsite was observed in the P4HS. Additionally, XRD patterns showed a clear increase in the intensity of kaolinite peaks from the DS to HS. These results support the hypothesis that the HS has more intense weathering conditions. In this case, in response to the higher precipitation values and strong leaching, desilication would have been responsible for the chemical migration of silica out of the solum, leading to the concentration of kaolinite (monosialitization), due to the more intense weathering environment (Papoulis et al. 2004; Samotoin and Bortnikov 2011). Sharper kaolinite peaks in the HS (when compared to the DS) provide further evidence of a more favorable environment for the occurrence of monosialitization. Additionally, kaolinite showed higher crystallinities in the HS profiles and in the P4DS profile, where weathering was likely stronger. XRD shoulders formed in the lower angles of P1DS, P2DS and P3DS evidence lower crystallinity of kaolinite in these profiles and, thus, a less favorable environment for monosialitization processes.

The presence of gibbsite in P4HS is probably related to its higher position within the slope and, thus, to a more

Table 4 Micromorphological characteristics of selected soil profiles

Depth (cm)	C/F ratio	C/F related distribution	Microstructure	Voids	Micromass	Pedofeatures
P1HS (368 m)—Haplic Alisol (Alumic, Rhodic) (Typic Rhodudult)						
21–31	1/2	Porphyric	Weakly developed subangular blocky	Vughs and channels	Reddish-yellow, undifferentiated	Clay coating
P4HS (846 m)—Haplic Cambisol (Alumic, Humic) (Oxic Dystrudept)						
18–28	1/3	Porphyric	Moderate developed subangular blocky (dominant) and granular	Vughs and channels	Reddish-yellow	External clay coating of aggregates (micropans)
P1DS (396 m)—Cutanic Luvisol (Epidystric, Rhodic) (Ultic Haplustalf)						
28–38	1/3	Porphyric	Weakly developed subangular blocky	Planar voids, vughs and chambers	Reddish-brown, striated b-fabric (porostriated)	Occasional textural pedofeatures: dense incomplete clay infillings
P4DS (823 m)—Haplic Acrisol (Chromic) (Typic Haplustult)						
36–46	1/2.5	Porphyric	Weakly developed subangular blocky and microgranular	Vughs and channels	Reddish-brown, striated b-fabric (granostriated) undifferentiated	Occasional textural pedofeatures: loose continuous clay infillings

intense degree of desilication (alitization or total desilication) at higher altitudes. In this case, gibbsite may have formed as an end product of kaolinite formation. Furian et al. (2002) and Herrmann et al. (2007) also indicated gibbsite as an important secondary mineral formed in places with high rainfall due to intense weathering processes, which indicates that altitudinal gradients may trigger an alitization process despite the semi-arid surrounding context. Bétard (2012) also found gibbsite in soils located at higher altitudes in the massif. In either case, gibbsite and kaolinite formation in the HS soils may have some role in the genesis of the clay-enriched subsurface horizons, which is in accordance with the higher mean clay contents in the HS (401 $\pm$ 84 %; for subsurface horizons) when compared to DS soils (319 $\pm$ 57 %; for subsurface horizons).

Contrastingly, in response to a drier and thus, less leached environment, bisialitization seemed to occur in the DS over more intense desilication processes, especially at lower altitudes (P1DS). In fact, XRD patterns of the P1DS profile, where the semi-aridity is more intense, showed the presence of 2:1 minerals with basal spacing at 1.40 nm, an observation also reported by Bétard (2012) for the same region. The semi-arid environment would have restricted silica (H_4SiO_4) and basic cations removal, favoring a partial desilication and the formation of 2:1 phyllosilicates. Less intense kaolinite peaks with respect to those registered at the HS soils and the presence of 2:1 clay minerals reinforces the less aggressive weathering conditions within this slope.

The neoformation of 2:1 minerals in the deeper layers of the DS soils may have been responsible for the genesis of the argic horizons (argillic according to Soil Taxonomy) and, thus, the textural differentiation between surface and subsurface horizons. In fact, Bétard et al. (2009) have evidenced illite neoformation, caused by weathering of feldspar crystals in Luvisols occurring in the semi-arid region of Baturité massif. In this case, the higher intensities of illite XRD peaks in DS soils may indicate that its genesis is favored in this pedoenvironment, at the expense of feldspars by neoformation (Bétard et al. 2009), or transformation of primary micas (Braga et al. 2002).

Micromorphological investigations

The profiles located at the lowest and highest elevations were chosen to carry out the micromorphological studies. In general, all profiles have porphyric distributions and a subangular blocky microstructure, showing different pedofeatures (summarized in Table 4). An important macromorphological difference that was observed between soils from both slopes was the identification (during profile description) of clay coatings only in DS soils, despite the presence of clay-enriched subsurface horizons in both slopes. However, based on the description of thin sections, these macromorphological features were not associated with pedofeatures indicators of clay illuviation (i.e., illuvial clay coatings). In this case, these macromorphological shiny surfaces would likely be related to an orientation of fine material (porostriated and granostriated b-fabrics; see Table 4; Fig. 4a), produced by tensional and compressional stresses induced by wetting and drying cycles, which are likely more frequent in the DS, due to the more contrasting seasonal variations. Additionally, the presence of high-activity clays in DS soils (as discussed below) may also have influenced the intensity of shrinking and swelling and, as a result, favored the genesis of shiny faces due the

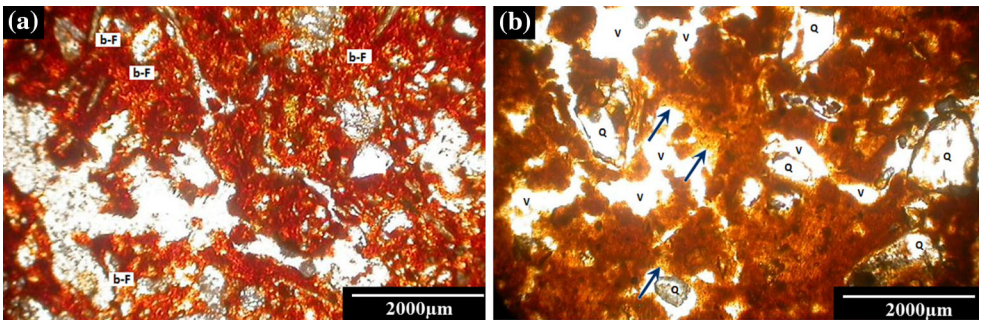

Fig. 4 Microphotographs of thin sections from selected soil horizons. Micromass from a subsurface soil horizon of the P1DS shows striated b-fabrics (b-F) XPL (**a**), and subsurface soil horizon of the P4HS shows the external coating of aggregates (micropans—*arrows*), PPL (**b**)

preferential orientation of clay minerals. In that case, the higher clay content in B horizons at the DS may have resulted from processes other than argilluviation (i.e., clay destruction in upper horizons, selective erosion of the surface layer and/or clay neoformation in the subsoil). However, the participation of clay illuviation in the genesis of the clay coatings in DS soils cannot be ruled out, since occasional textural pedofeatures (both dense and loose clay infillings; see Table 4) were described in different thin sections of its soils.

Contrastingly, despite the absence of clay coating observed in the field, thin sections from HS soils showed more evident textural pedofeatures (clay coatings), likely related to argilluviation (Table 4; Fig. 4b). In this case, argilluviation may have been partially responsible for the textural contrasts. Since most of these textural pedofeatures were non-laminated, poorly orientated and with absent extinction lines, the participation of other mechanisms in the genesis of argic horizons (argillic according to Soil Taxonomy) from the HS cannot be discarded. Additionally, it must be considered that processes such as iron segregation, and soil swelling and shrinking (due to the presence of high-activity clays, Fig. 2) may alter the micromorphological patterns of the textural pedofeatures.

Conclusions

The contrasting climatic conditions imposed by the elevational gradient and orientation of Baturité massif have triggered, within a semi-arid context, the occurrence of pedogenetic processes typical of tropical wet conditions, such as melanization, brunification, alitization, intense lixiviation and acidification. The more humid pedoenvironment at the HS has clearly intensified these processes, which also increased in intensity with altitude. Although most soils, irrespective of the slope, have presented clay-enriched subsurface horizons, results indicate a minor participation of clay illuviation, mainly in dry slope soils (DS). Even though present in low amounts in most semi-arid soils, iron oxide distribution still presented itself as an important indicator of the different pedoenvironments.

References

Ab'Saber AN (1977) Os domínios morfoclimáticos na América do Sul: primeira aproximação. USP, São Paulo

Barbiéro L, Cunnac S, Mané L, Laperrousaz C, Hammecker C, Maeght JL (2001) Salt distribution in the Senegal middle valley analysis of a saline structure on planned irrigation schemes from N'Galenka creek. Agr Water Manag 46:201–213

Bétard F (2012) Spatial variations of soil weathering processes in a tropical mountain environment: the Baturité massif and its piedmont (Ceará, NE Brazil). Catena 93:18–28

Bétard F, Peulvast JP, Sales VC (2007) Caracterização morfopedólogica de uma serra úmida no semi-árido do nordeste brasileiro: o caso do maciço de Baturité-CE. Mercator 6:107–126

Bétard F, Caner L, Gunnell Y, Bourgeon G (2009) Illite neoformation in plagioclase during weathering: evidence from semi-arid Northeast Brazil. Geoderma 152:53–62

Bockheim JG, Munroe JS, Douglass D, Koemer D (2000) Soil development along an elevational gradient in the southeastern Uinta Mountains, Utah, USA. Catena 39:169–185

Boero V, Schwertmann U (1989) Iron oxide mineralogy of terra rossa and its genetic implications. Geoderma 44:319–327

Braga MA, Paquet H, Begonha A (2002) Weathering of granites in a temperate climate (NW Portugal): granitic saprolites and arenization. Catena 49:41–56

Brock-Hon AL, Robins CR, Buck BJ (2012) Micromorphological investigation of pedogenic barite in Mormon Mesa petrocalcic horizons, Nevada USA: implication for genesis. Geoderma 179–180:1–8

Bullock P, Fedoroff N, Jongerius A, Stoops G, Tursina T (1985) Handbook for soil thin section description. Waine Research Publications, Wolverhampton

Chen T, Xie Q, Xu H, Chen J, Ji J, Lu H, Balsam W (2010) Characteristics and formation mechanism of pedogenic hematite in Quaternary Chinese loess and paleosols. Catena 81:217–225

Egli M, Mirabella A, Sartori G, Zanelli R, Bischof S (2006) Effect of north and south exposure on weathering rates and clay mineral formation in Alpine soils. Catena 67:155–174

Egli M, Mirabella A, Sartori G (2008) The role of climate and vegetation in weathering and clay mineral formation in late Quaternary soils of the Swiss and Italian Alps. Geomorphology 102:307–324

Egli M, Sartori G, Mirabella A, Favilli F, Giaccai D, Delbos E (2009) Effect of north and south exposure on organic matter in high Alpine soils. Geoderma 149:124–136

Embrapa—Brazilian Agricultural Research Corporation (2011) Manual de Métodos de Análise de Solo. Embrapa, Rio de Janeiro

Embrapa—Brazilian Agricultural Research Corporation (2013) Sistema Brasileiro de Classificação de Solos. Embrapa, Rio de Janeiro

Etame J, Gerard M, Suh CE, Bilong P (2009) Halloysite neoformation during the weathering of nephelinitic rocks under humid tropical conditions at Mt Etinde, Cameroon. Geoderma 154:59–68

Fitzpatrick RW, Schwertmann U (1982) Al-substituted goethite—an indicator of pedogenic and other weathering environments in South Africa. Geoderma 27:335–347

Furian S, Barbiéro L, Boulet R, Curmi P, Grimaldi M, Grimaldi C (2002) Distribution and dynamics of gibbsite and kaolinite in an oxisol of Serra do Mar, southeastern Brazil. Geoderma 106:83–100

Gee GW, Bauder JW (1986) Particle-size analysis. In: Klute A (ed) Methods of soil analysis part 1 physical and mineralogical methods, 2nd edn. SSSA Book Series, Madison, pp 383–411

Herrmann L, Anongrak N, Zarei M, Schuler U, Spohrer K (2007) Factors and processes of gibbsite formation in Northern Thailand. Catena 71:279–291

IUSS Working Group WRB (2006) World reference base for soil resources: a framework for international classication, Correlation and Communication. FAO, Rome

Jacomine PKT, Almeida JC, Medeiros LAR (1973) Levantamento Exploratório-Reconhecimento de solos do Estado do Ceará. Ministério da Agricultura, Recife

Kaiser K, Guggenberger G (2007) Sorptive stabilization of organic matter by microporous goethite: sorption into small pores vs. surface complexation. Eur J Soil Sci 58:45–59

Kämpf N, Schwertmann U (1982) Goethite and hematite in a climosequence in southern Brazil and their application in classification of kaolinitic soils. Geoderma 29:27–39

Khormali F, Ajami M (2011) Pedogenetic investigation of soil degradation on a deforested loess hillslope of Golestan Province, Northern Iran. Geoderma 167–168:274–283

Mehra OP, Jackson ML (1960) Iron oxide removal from soils and clays by adithionite-citrate system buffered with sodium bicarbonate. Clay Clay Miner 7:317–327

Moore DM, Reynolds RC (1997) X-ray diffraction and the identification and analysis of clay minerals. Oxford University Press, Oxford

Motta PEF, Kämpf N (1992) Iron oxide properties as support to soil morphological features for prediction of moisture regimes in Oxisols of Central Brazil. Z Pflanz Bodenkunde 155:385–390

Murad E, Wagner U (1994) The Mössbauer spectrum of illite. Clay Miner 29:1–10

Murphy CP (1986) Thin section preparation of soils and sediments. AB Academic Publishers, Berkhamsted

Oliveira AP, Ker JC, Silva IR, Fontes MPF, de Oliveira AP, Neves ATG (2010) Spodosols pedogenesis under Barreiras formation and sandbank environments in the south of Bahia. R Bras Ci Solo 34:847–860

Papoulis D, Tsolis-Katagas P, Katagas C (2004) Progressive stages in the formation of kaolin minerals of different morphologies in the weathering of plagioclase. Clay Clay Miner 52:275–286

Quaggio JA, van Raij B, Mallavolta E (1985) Alternative use of the SMP-buffer solution to determine lime requirement of soils. Commun Soil Sci Plan 16:245–260

Rech JA, Reeves RW, Hendricks DM (2001) The influence of slope aspect on soil weathering processes in the Springerville volcanic field, Arizona. Catena 43:49–62

Samotoin ND, Bortnikov NS (2011) Formation of kaolinite nano and microcrystals by weathering of phyllosilicates. Geol Ore Depos 53(4):340–352

Sampaio EVSB (1995) Overview of the Brazilian caatinga. In: Bullock SH, Mooney HA, Medina E (eds) Seasonally dry tropical forests. Cambridge University Press, New York, pp 34–63

Schwertmann U (1966) Inhibitory effect of soil organic matter on the crystallization of amorphous ferric hydroxides. Nature 212:645–646

Schwertmann U (2008) Iron oxides. In: Chesworth W (ed) Encyclopedia of soil science. Springer, Dordrecht, pp 363–369

Schwertmann U, Wagner F, Knicker H (2005) Ferrihydrite-humic associations: magnetic hyperfine interactions. Soil Sci Soc Am J 69:1009–1015

Silva VPR (2004) On climate variability in Northeast of Brazil. J Arid Environ 58:575–596

Soil Survey Staff (2014) Keys to soil taxonomy, 12th edn. USDA-Natural Resources Conservation Service, Washington, DC

Souza MJN (1994) Geossistemas e potencialidades dos recursos naturais: Serra de Baturité e áreas sertanejas periféricas. FUNCEME, Fortaleza

Souza FP, Ferreira TO, Mendonça ES, Romero RE, Oliveira JGB (2012) Carbon and nitrogen in degraded Brazilian semi-arid soils undergoing desertification. Agr Ecosyst Environ 148:11–21

Stoops G (2003) Guidelines for analysis and description of soil and regolith thin sections. SSSA Book Series, Madison

Tardy Y (1971) Characterization of the principal weathering types by the geochemistry of waters from some European and African crystalline massifs. Chern Geol 7:253–271

Torrent J, Guzman R, Parra MA (1982) Influence of relative humidity on the crystallization of Fe(III) oxides from ferrihydrite. Clay Clay Miner 30:337–340

Yousefifard M, Ayoubi S, Jalalian A, Khademi H, Makkizadeh MA (2012) Mass balance of major elements in relation to weathering in soils developed on igneous rocks in a semi-arid region, northwestern Iran. J Mt Sci 9:41–58